PCCP

Cite this: *Phys. Chem. Chem. Phys.*, 2011, **13**, 1762–1769

www.rsc.org/pccp

PAPER

Temperature-cycle single-molecule FRET microscopy on polyprolines

Haifeng Yuan,[a] Ted Xia,†[a] Benjamin Schuler[b] and Michel Orrit*[a]

Received 10th September 2010, Accepted 11th November 2010
DOI: 10.1039/c0cp01772h

Accessing the microsecond dynamics of a single fluorescent molecule in real time is difficult because molecular fluorescence rates usually limit the time resolution to milliseconds. We propose to apply single-molecule temperature-cycle microscopy to probe molecular dynamics at microsecond timescales. Here, we follow donor and acceptor signals of single FRET-labeled polyprolines in glycerol to investigate their conformational dynamics. We observe a steady-state FRET efficiency distribution which differs from theoretical distributions for isotropically orientated fluorescent labels. This may indicate that the orientation of fluorescent labels in glycerol is not isotropic and may reflect the influence of the dye linkers. With proper temperature-cycle parameters, we observed large FRET changes in long series of cycles of the same molecule. We attribute the main conformational changes to reorientations of the fluorescent labels with respect to the oligopeptide chain, which take place in less than a few microseconds at the highest temperature of the cycle (250 K). We were able to follow the FRET efficiency of a particular construct for more than 2000 cycles. This trajectory displays switching between two conformations, which give rise to maxima in the FRET efficiency histogram. Our experiments open the possibility to study biomolecular dynamics at a time scale of a few microseconds at the single-molecule level.

1. Introduction

Since the first single molecule fluorescence detection,[1] single-molecule techniques have been widely used for many chemical and biological studies because they suppress ensemble averaging and give access to rare species and intermediate states.[2] Among all the single-molecule fluorescence techniques, single-pair fluorescence resonance energy transfer (sp-FRET), first demonstrated by Ha *et al.*,[3] has become a powerful tool for probing molecular interactions and dynamics. It is widely applied for structural and dynamics studies on biological molecules such as DNA, RNA and proteins.[3–13] Fluorescence resonance energy transfer is the process by which energy absorbed by one fluorophore (the donor) is transferred to another fluorophore (the acceptor) with a lower excitation energy. FRET proceeds *via* dipole–dipole interaction and requires that the donor's fluorescence spectrum overlaps with the absorption spectrum of the acceptor. The rate of energy transfer scales as the sixth power of the distance between the two dipoles.[14] According to Förster's theory, the energy transfer efficiency E can be expressed by the following equation:

$$E = \frac{1}{1 + \left(\frac{R}{R_0}\right)^6} \quad (1)$$

where the Förster radius R_0, which is the distance corresponding to 50% energy transfer, is defined with[14]

$$R_0^6 = \frac{9000 Q_D (\ln 10)\kappa^2 \int f_D(\lambda)\varepsilon_A(\lambda)\lambda^4 d\lambda}{128\pi^5 n^4 N_A} = C\kappa^2 \quad (2)$$

In eqn (2), constant C depends only on the photophysical properties of the donor and acceptor and on the medium. Q_D is the quantum yield of the donor, $f_D(\lambda)$ is the normalized emission spectrum of the donor as a function of wavelength λ and $\varepsilon_A(\lambda)$ is the normalized absorption spectrum of the acceptor. The orientation factor κ^2 gives the dependence of the interaction between the two electric dipoles on their orientations and respective positions. In many cases one assumes that both donor and acceptor can freely rotate and one replaces κ^2 by its dynamically averaged value of 2/3.[15,16] Thus, FRET can be used for extracting distance information and for probing molecular interactions or conformational changes at nanometre scales.[14] In single-molecule FRET experiments, doubly labeled molecules are either freely diffusing in solution or immobilized. In the former scheme, a confocal microscope is employed to detect photon bursts when the molecule diffuses through the detection volume. Measuring the fluorescence intensities of donor and acceptor, one

[a] *Molecular Nano-Optics and Spins, Leiden Institute of Physics, Leiden University, Leiden, The Netherlands. E-mail: orrit@molphys.leidenuniv.nl*
[b] *Biochemisches Institut, University of Zurich, Zurich, Switzerland*
† Present address: Institute of Chemistry, Chinese Academy of Science, Beijing, China.

calculates the FRET efficiency for each burst, whence one extracts the associated distribution as a histogram. However, due to the limited dwell time of the molecules in the detection volume, dynamics on timescales longer than the characteristic diffusion time of the molecule are not accessible. Even for immobilized molecules, it is not possible to observe the same FRET pair for long times because of photobleaching of the fluorophores. Photobleaching is a photochemical process by which a fluorophore goes into a non-absorbing or non-fluorescing form. Therefore, standard single-molecule fluorescence techniques cannot access long times. Similarly, the access to times shorter than milliseconds is limited by the rate at which a single molecule emits photons.

Biological processes, however, cover a very broad range of times. For instance, protein folding involves dynamics ranging from nanoseconds to hours.[17] The temperature-cycle method was developed to extend the time range accessible to single-molecule fluorescence measurements.[18] This method is related to the temperature-jump measurements applied to biomolecules at room temperature, which is already well established and widely used.[19,20] In our temperature-cycle setup, a small sample region (approximately 1 μm diameter) around the molecule of interest experiences fast temperature cycles. The lower temperature is maintained by a cryostat and a higher temperature is reached by optical heating of the small sample region. The extreme temperatures are chosen such that the dynamics of interest will be frozen at the lowest temperature and activated at the highest temperature. The highest temperature and the dwell time during each cycle can be chosen and controlled according to the dynamical processes studied. A dynamical process can thus be studied as a consecutive series of snapshots of frozen states. By recording the series of FRET snapshot signals, we can reconstruct any conformational dynamics, the time resolution being limited only by the cooling and heating times (typically around 4 microseconds[18]). To keep these times as short as possible, we have to limit the size of the heated sample area. Heating is achieved by focusing a continuous wave near-infrared (NIR) laser beam on the surface of an absorbing metal film (chromium), which serves as a substrate for the sample. The time needed to heat or cool the focal volume is determined by heat diffusion and is of the order of a few microseconds. The temperature cycles are applied to a single molecule in the focus by means of a sequence of heating and excitation periods as shown in Fig. 1.

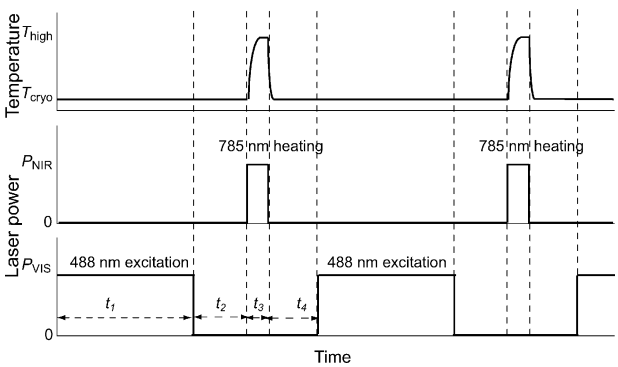

Fig. 1 Scheme of the temperature-cycle method. The top curve represents the temperature in the NIR heating focal volume; the curve in the middle represents the on- and off-times of the NIR heating beam; the bottom curve represents the on- and off-times of the excitation laser beam. t_1 is the duration during which the excitation is applied; t_2 and t_4 are the delay time inserted in between excitation and heating; t_3 is the heating duration.

Hereafter, we briefly explain how we hope to reconstruct conformational dynamics by a series of snapshot structures. We assume that any molecular dynamics or evolution (slower than microseconds) is completely suppressed during the cold periods, as well as during the short cooling and heating times. We can then see the successive hot periods as seamlessly connecting to one another. If all intervening dynamics have been suspended, the next hot period resumes evolution exactly where the previous one left it. Therefore, the successive structures recorded during the low-temperature times amount to instantaneous snapshots of the reconstructed high-temperature evolution, as if the hot periods had succeeded continuously. This is only possible if assuming that the whole memory of the previous structure is perfectly conserved upon fast cooling.

2. Materials and methods

2.1 The sample

Here we use an oligopeptide (type-II polyproline) as an example of a temperature-cycle study of conformational dynamics of a single molecule. Polyprolines were first used for demonstrating FRET as a "molecular ruler" by Stryer and Haugland[21] and revisited using smFRET by Schuler *et al.*[7] Type-II polyproline has a relatively rigid structure and has a persistence length of 13 nm.[35] 6-Residue polyproline has a contour length of 1.8 nm and 20-residue polyproline has a contour length of 6 nm. The polyprolines labeled with Alexa488 as the donor and Alexa594 as the acceptor are the same as those used by Schuler *et al.*[7] In this work, we use polyproline-6 and polyproline-20 to represent the FRET-labeled 6-residue and 20-residue polyproline constructs respectively. The molecular structure of polyproline-6 is shown in Fig. 2.

We choose glycerol as the solvent in our experiment for several reasons. Firstly, glycerol is not harmful to proteins and is often used to protect proteins at low temperature[22,23] or

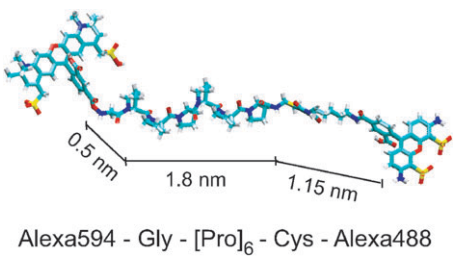

Fig. 2 The molecular structure of polyproline-6 labeled with Alexa488 as the donor and Alexa594 as the acceptor. The donor dye (Alexa488) is conjugated to the carboxyl-terminal cysteine residue by a five-carbon link (approximately 0.9 nm), which is longer than the two-carbon link used to attach the acceptor (Alexa594) to the amino-terminal glycine.

improve their thermal stability.[24] Even though glycerol is known as a crowding agent and an osmolyte,[25,26] the conformational distribution of polyproline is not expected to be strongly affected by glycerol.[27] Secondly, glycerol is very viscous at room temperature (about a thousand times more viscous than water) and can form a stable liquid film on a glass surface. Its viscosity varies by about 10 orders of magnitude from room-temperature to the glass transition (190 K),[22,28] a property which can be used for temperature jump calibration.[18] In addition, the low evaporation rate of glycerol makes it easier to prepare and handle thin films.

2.2 Experimental set-up

The setup combines a low-temperature home-built single-molecule confocal microscope and a heating path for the fast temperature cycles. It has been described in detail in previous work by Zondervan *et al*.[18] The optical path around the sample in the cryostat is shown in Fig. 3. The NIR heating beam from a 785 nm single-mode diode laser (TOPTICA Photonics AG) enters the cryostat through one of its side windows. It is directed downward by a mirror and focused onto the chromium film by an aspheric singlet lens (NA = 0.68). Three degrees of freedom for the sample plate and one for the NIR lens are actuated by four inchworm motors (Attocube) held by a home-built cryostat insert. The two additional degrees of freedom needed to bring the focus of the NIR lens in coincidence with the focus of the objective lens are actuated by a steering mirror on the NIR beam outside the cryostat. Thus, this insert allows us to overlap the visible and NIR foci and to bring the molecule of interest into this common focus. Two additional lateral adjustments are provided by a scanning mirror on the visible path of the confocal microscope. The excitation beam, either the 488 nm beam from an Argon-ion laser (Spectra-Physics) or the 594 nm beam from a He–Ne laser (Melles Griot) was circularly polarized. It enters the cryostat through the bottom window and is focused by a custom-made low temperature microscope objective (NA = 0.85, Bernhard Halle) onto the sample surface. The fluorescence emitted from the sample is collected

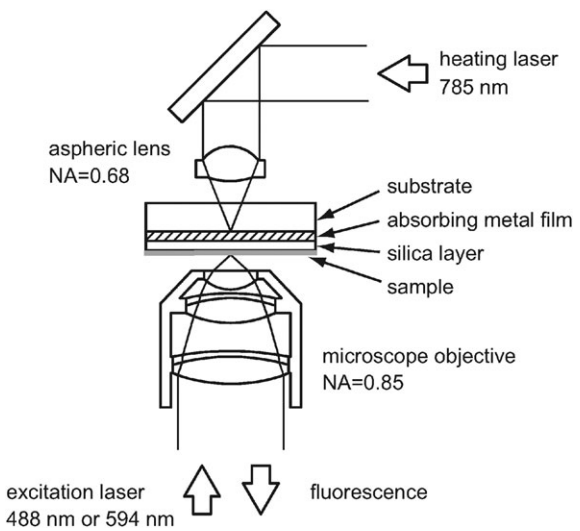

Fig. 3 Scheme of the optical set-up inside the cryostat.

with the same objective and sent, without polarization analysis, to detection through the bottom window of the cryostat.

Outside the cryostat, the collected fluorescence passes through a 100 μm pinhole, then it passes through a set of filters to remove the scattered laser light (Semrock NF01-488U-25 and LP02-488RU-25 for the 488 nm laser, NF01-594U-25 for the 594 nm laser, and Thorlabs FES0700, a shortpass filter for blocking the NIR heating laser). A dichroic mirror (585DCXR, AHF Analysentechnik) separates the fluorescence into the donor detection and the acceptor detection channels. In the donor fluorescence detection channel, a bandpass filter (HQ535/50X, AHF Analysentechnik) is used to select the fluorescence photons from the donor fluorophore. In the acceptor channel, a longpass filter (HQ615LP) and a bandpass filter (HQ638/95M) are applied to select the fluorescence photons from the acceptor fluorophore. In both channels, the beams are focused onto photon-counting avalanche photodiodes (SPCM-AQR, Perkin-Elmer).

The laser beams are modulated with two acousto-optical modulators (AA Opto-Electronic). The alternating scheme shown in Fig. 1 is controlled by the ADwin-Gold system (Jäger Computergesteuerte Messtechnik GmbH) *via* our data-acquisition program written in Labview.

2.3 Sample preparation

The dual-labeled polyprolines were dissolved at a concentration of 10^{-12} M in 50 mM sodium phosphate solution (the pH was adjusted to 7.0) with 0.001% of Tween20 to prevent surface adhesion of the polypeptides. Glycerol was finally added to this solution at a 1 : 1 volume ratio. The glycerol solution was directly spin-coated at 6000 rpm on the glass slides. The excess water evaporated upon or after spin-coating, leaving a nearly pure glycerol film. The slides were 20 mm round microscope slips coated with 50 nm of chromium and a protective layer of 50 nm silica to isolate the polyprolines and the fluorophores from the metal. Before spin-coating, the substrates were treated in a UV-ozone cleaner (model 42-220, Jelight, Irvine, CA) for two hours. The resulting thickness of the glycerol film from this procedure was around 0.5–2 μm, as deduced from examination in a home-built Michelson interferometer. We subsequently dried the samples in the cryostat by repeatedly pumping and flushing with helium gas and kept them under dry helium throughout all experiments.

2.4 Heating calibration

For calibrating the heating temperature on the metal film in the focal volume, we followed the method used in the work of Zondervan and coworkers.[18] The fluorescence anisotropy of Rhodamine 6G in glycerol shows a marked increase in the temperature range from 200 to 280 K. This effect allowed us to calibrate the temperature in the center of the heating spot from the fluorescence anisotropy of Rhodamine 6G (10^{-5} M) in glycerol as a function of NIR power in a series of images at varying heating power. The resulting local temperature calibration is shown in Fig. 4 where a linear fit gives a slope

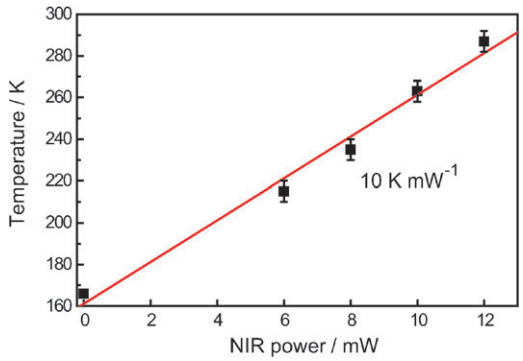

Fig. 4 Temperature in the NIR heating focal volume calibrated by fluorescence anisotropy of Rhodamine 6G in glycerol with different NIR heating powers.

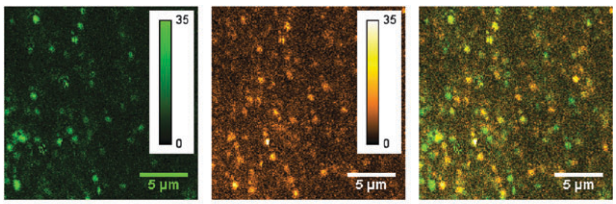

Fig. 5 Scanning images of dual-labeled polyproline-6 at 170 K on an area of 20 × 20 μm^2 with a pixel step of 100 nm and an excitation intensity of 2.0 kW cm^{-2}. (a) Donor fluorescence image; (b) acceptor fluorescence image; (c) superposition of (a) and (b).

of 10 K mW^{-1}, which is in good agreement with the previous calibration (10.3 K mW^{-1}).[18]

2.5 Data analysis

Images, as shown in Fig. 5, were obtained by scanning a sample area of 20 × 20 μm^2 with a pixel step of 100 nm, an excitation intensity of 2.0 kW cm^{-2}, and an acquisition time of 10 ms. We alternate the laser sources of 488 and 594 nm respectively. By doing this, we can check which molecules are full constructs with both Alexa488 and Alexa594 dyes; moreover, we can tell whether the disappearance of the acceptor fluorescence signal during a time trace measurement is due to photoblinking or bleaching from comparing the 594 nm excitation scanning image before and after measuring a fluorescence time trace. In our data analysis, we only considered the molecules for which both dyes were detectable.

The FRET efficiency can be measured by determining the donor lifetime or its fluorescence intensity in the presence and absence of the acceptor. Alternatively, here it is calculated with

$$E = \frac{I_A}{I_A + \gamma I_D}. \quad (3)$$

In this equation, I_A is the fluorescence intensity from the acceptor, and I_D is the fluorescence intensity from the donor. γ is a parameter correcting for the photophysics properties of the fluorophores, $\gamma = \frac{\Phi_A \eta_A}{\Phi_D \eta_D}$. Φ_A and Φ_D are the quantum yields of the acceptor and the donor, η_A and η_D are the detection efficiency of the acceptor and the donor.[3] The quantum yields of the dyes depend on their surroundings.[14] Hence, the quantum yields could be slightly different for each single construct. Moreover, both the absorption and emission of the fluorophores are polarization dependent. Thus, although the excitation was circularly polarized, the orientation of the dyes also influences the fluorescence detection efficiency in solid-phase single-molecule optical experiments, as reported elsewhere.[29–31] In this work, we neglected this dependence and used an orientation-averaged γ estimated to about 1.0. A Labview-based analysis routine was used to facilitate automatic FRET calculation from the raw intensity traces recorded with temperature cycles. For the steady-state measurement, the FRET efficiencies are calculated using the averaged fluorescence of recorded time traces. For the temperature-cycle measurements, the data were sampled synchronously with 488 nm excitation, and only those with signals above a set threshold were taken into account.

3. Results and discussions

3.1 Steady-state measurements

We first present our results of steady-state spFRET measurements of dual-labeled polyproline-6 and polyproline-20. We kept the temperature in the cryostat at 170 K which is below the glass transition temperature of glycerol (190 K),[22,28] so the molecules are immobilized.

Room-temperature single-molecule FRET measurements usually show anti-correlation between the donor and the acceptor channels. Here, on the contrary, we observe mostly correlated changes in the donor and acceptor channels, as shown in Fig. 6(b), (c) and (e). Only a few traces, like trace (d), show anti-correlated changes. We attribute the correlation between donor and acceptor channels to photophysics of the donor. We expect both fluorophores to present blinking events similar to those of Rhodamine 6G in glycerol, because they have closely related structures.[32,33] In particular, transition of the donor to a dark state will interrupt energy transfer to the acceptor. Similarly, a dark state of the acceptor could lead to

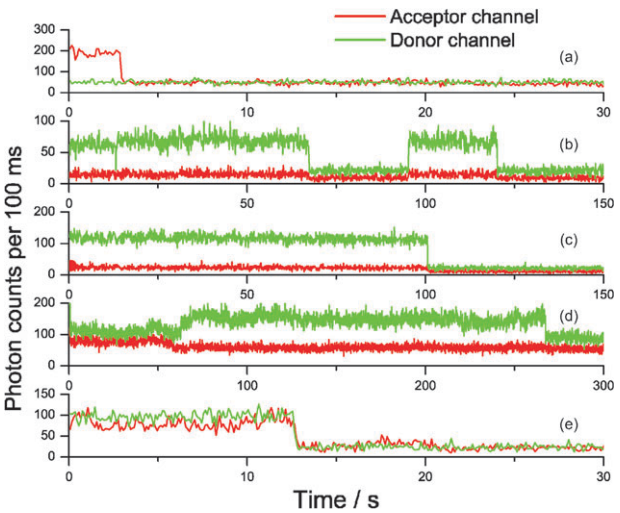

Fig. 6 Time traces of five different molecules of dual-labeled polyproline-6 with an excitation intensity of 1.0 kW cm^{-2}, and an acquisition time of 100 ms at 170 K.

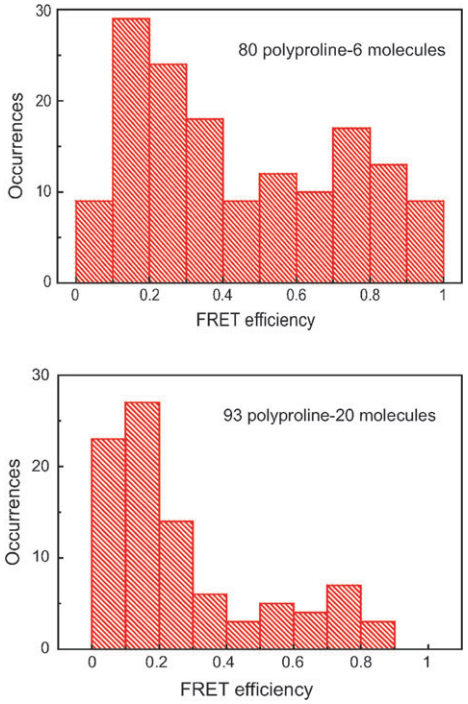

Fig. 7 Steady-state FRET efficiency histograms of dual-labeled polyproline-6 (the top one), polyproline-20 (the bottom one). The FRET efficiencies are calculated from the recorded fluorescence time traces with the methods mentioned above; all the measurements are made at 170 K with 488 nm excitation intensity 1.0 kW cm^{-2} and an acquisition time of 100 ms.

an increase of the donor fluorescence if the dark acceptor state does not absorb the donor emission. However, this was very rarely observed, which indicates that the dark state of the acceptor can still quench the donor fluorescence. This quenching can also occur when the acceptor is bleached, as trace (a) in Fig. 6 shows.

The average FRET efficiency is calculated for each fluorescence trace and taken into the histograms shown in Fig. 7. Both histograms show very broad distributions and a large population of low energy transfer efficiency. Note that efficiencies lower than 0.05 cannot be reliably estimated because of background and have been omitted from the histograms. The obtained distributions are very different from those at room temperature in water solution, which are narrow and, for polyproline-6, peak at a high FRET efficiency.[7,34] Compared to polyproline-6, polyproline-20 has an even bigger population at the low FRET efficiency region, which is obviously related to the longer distance between the two fluorophores.

As we mentioned in the Introduction, the FRET rate depends on intramolecular distance and on the dipole orientations. In most room-temperature experiments, the distribution of FRET efficiencies provides information about the donor–acceptor distance because their reorientation in liquid solution is very fast, leading to the averaged orientation factor. In our case, the molecular constructs are embedded in a glassy matrix. The spacer is stiff and the orientations of the fluorophores are frozen. There is thus no averaging of the orientation factors during each measurement,

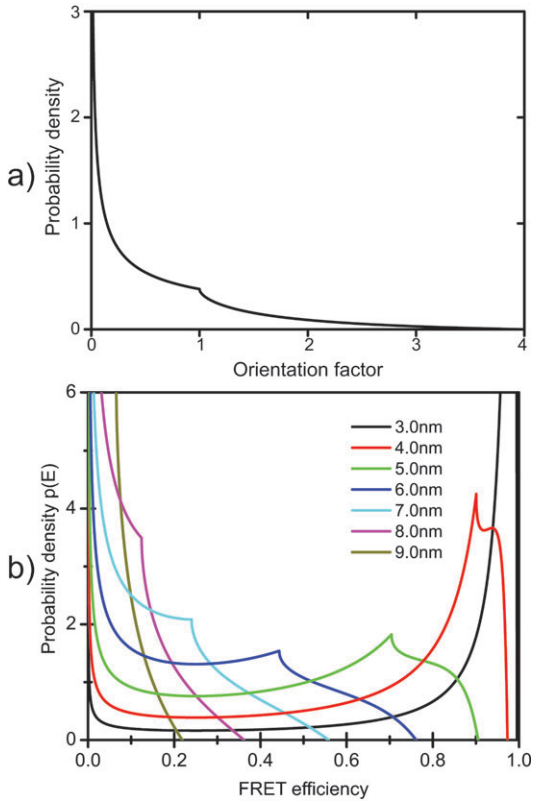

Fig. 8 (a) Theoretical probability density of the orientation factor for isotropically random oriented dipoles.[15] (b) The probability density distribution of the FRET efficiency with an assumed series of rigid distances between the two dipoles, and static, but random relative orientation of donor and acceptor.

and the orientation factor κ^2 in eqn (2) becomes a distributed variable. The probability distribution of the orientation factor κ^2 has been evaluated theoretically for the case of isotropic distributions of donor and acceptor dipoles in the work of Dale *et al.*[15] This distribution, shown in Fig. 8(a), is given by:[7,15]

$$P(\kappa^2) = \begin{cases} \frac{1}{2\sqrt{3\kappa^2}} \ln(2+\sqrt{3}), & 0 \le \kappa^2 \le 1 \\ \frac{1}{2\sqrt{3\kappa^2}} \ln\left(\frac{2+\sqrt{3}}{\sqrt{\kappa^2}-\sqrt{\kappa^2-1}}\right), & 1 \le \kappa^2 \le 4 \end{cases} \quad (4)$$

This probability density of the FRET efficiency E can be calculated from κ^2 according to eqn (1), (2) and (4). The corresponding histograms for various FRET distances are presented in Fig. 8(b).[7]

Assuming that the interdye distances are 3 nm for polyproline-6 and 7 nm for polyproline-20, we expect FRET efficiency distributions similar to the 3 nm and 7 nm curves in Fig. 8(b) for polyproline-6 and polyproline-20 respectively. However, the measured FRET distribution of polyproline-6 clearly differs from the theoretical distribution of Fig. 8(b) (the black curve). The large probability of near-total FRET is absent, and we find a large population of molecules with FRET efficiencies lower than 0.6. These two features may indicate that the orientational distributions of donor or acceptor are not isotropic, and they may also be affected by the sampling of larger distances due to the dye linkers. The experimental FRET distribution of polyproline-20 has a large

population of conformations with a low FRET efficiency. But, contrary to the predicted 7 nm curve, it still has conformations with FRET efficiencies higher that 0.6, which may indicate that the inter-dye distance in at least part of the polyproline-20 constructs is actually lower than 7 nm. We attribute this effect to the flexible linkers, which allow the dyes to approach to shorter distances.[35]

3.2 Temperature-cycle measurements

The temperature-cycle measurements are carried out with the scheme of Fig. 1. The illumination sequence is: excitation at 488 nm for duration t_1, delay time t_2, NIR heating for duration t_3 and delay time t_4. The delays of a few milliseconds are inserted to entirely separate the two beams and to allow for more time for temperature stabilization. The characteristic times of the temperature changes are on the order of a few microseconds.[18] As we noticed, the orientation of the fluorophores plays an important role in FRET measurements and leads to a FRET distribution which disagrees with the expected isotropic distribution. Indeed, the reorientation of the free dyes in glycerol occurs on a timescale of microseconds at 250 K. We therefore expect to observe FRET changes due to dye reorientation if we set the highest temperature in the cycles to 250 K.

Hence, we made use of the dye reorientation to demonstrate the temperature-cycle method in this work. In the following, the conformation changes we refer to are reorientations of the fluorophores in the FRET-labeled polyproline constructs. Here, we applied a 300 ms excitation/observation time (t_1), 50 ms delay time (t_2, t_4) and a 10 μs heating time (t_3) with 10 mW NIR power. This power brings the heated volume approximately 80 K above the cryostat's temperature (170 K) within 10 μs. This resulting temperature (250 K) should be high enough to see the FRET efficiency change due to reorientation of the fluorophores. The results shown in Fig. 9(a) and (b), however, indicate different behavior. The FRET efficiencies often remain approximately constant for several cycles. In the upper trace of Fig. 9(a), the FRET efficiency fluctuated around 0.3 in the first 14 cycles, and then underwent a sudden change to a higher value of 0.8. After the jump, the efficiency varied considerably more after each temperature cycle, until the acceptor bleached and the donor fluorescence increased before bleaching in its turn. In the other trace of Fig. 9(a), the FRET construct stayed a long time with a fairly low FRET efficiency around 0.4, then went to a high FRET efficiency around 0.9 until both of the donor and the acceptor turned dark. These changes of the FRET efficiency are presumably due to reorientation of the fluorophores rather than to conformation changes of the peptide chain.

In order to follow the same molecule for longer time with more temperature cycles, we shortened the excitation/observation time to a few milliseconds. A reconstructed temperature-cycle FRET trace from one single polyproline-6 construct is shown in Fig. 9(b). This construct experienced more than 2600 temperature cycles between 170 and 250 K. The donor and the acceptor gave anti-correlated fluorescence signals, with thirteen sudden jumps between two main conformations during the measurement time. In the absence

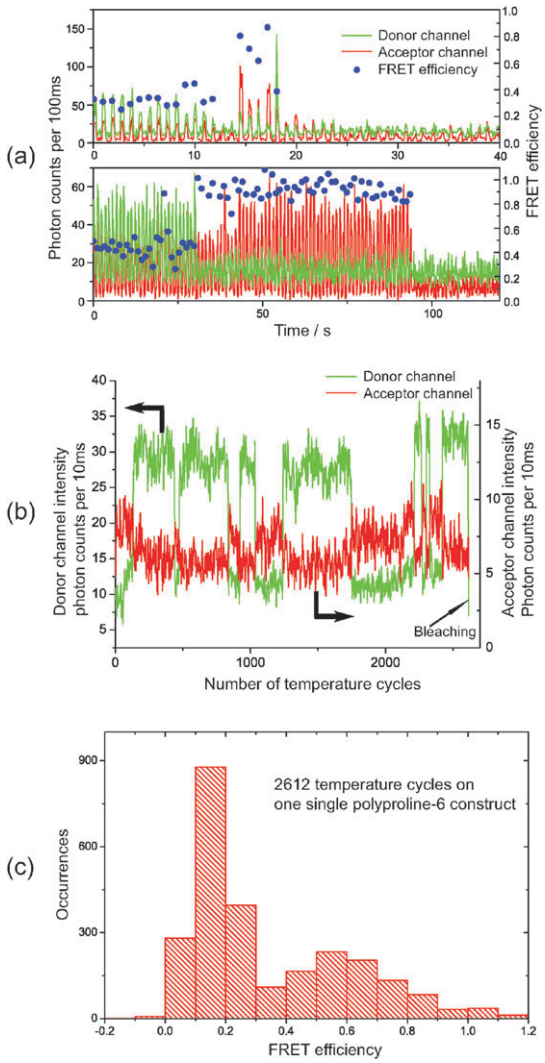

Fig. 9 (a) Raw temperature-cycle time traces of polyprolin-6 on two different molecules. The green and red traces represent the fluorescence signals from the donor and the acceptor respectively; and the blue dots are the calculated FRET efficiencies. The peaks of the traces are recorded during the excitation and the lower levels are dark counts from the APDs during the delay time and heating time. (b) A trace reconstructed from a polyproline-6 molecule which experienced more than 2600 temperature cycles between 170 and 250 K. Contrary to (a), only the excitation and measurement part of the cycles are indicated. (c) FRET histogram from (b). The FRET values below 0 and beyond 1 are due to noise and to background subtraction in data analysis.

of information on the orientations of donor and acceptor, we cannot discriminate contributions to these jumps from distance changes and orientation changes. An efficiency histogram of this trace is shown in Fig. 9(c). The FRET efficiency distribution, although broad, presents two maxima, which can be attributed to the two main conformations of Fig. 9(b).

We now comment on the different reorientation behavior of the tethered dyes compared to the free dyes. At 250 K, the free dyes tumble on a time scale of microseconds. The tethered dyes, in contrast, remain fixed for many temperature cycles, amounting to a dwell time of milliseconds at the highest temperature of 250 K. We can propose several explanations for this near-absence of reorientations. The constructs could

stick at the surface of the solid slide. We think this unlikely, as all studied molecules (more than 30 in different sample areas) behaved in the same way. They all maintained an almost constant FRET efficiency with small fluctuations for many temperature cycles. Some of them had a few sudden FRET efficiency jumps, while the others presented a constant FRET efficiency until photobleaching occurred. A second possibility is that the dyes are blocked by their interaction with the polypeptide chain. This marked difference from water solution at room temperature could arise from the lower temperature or from the special structure of glycerol. Indeed, glycerol has a complex behavior close to the glass transition.[36–42] Glycerol forms a highly cross-linked network of hydrogen bonds,[41] which reduces the mobility of glycerol and dye molecules as well as that of the constructs. Yet another possibility is that the glycerol structure is altered in the vicinity of the peptide chain, blocking the reorientation of the dyes, even at the comparatively high temperature of 250 K. Furthermore, the different linkers for the donor and acceptor dyes can make the reorientation properties of the donor and the acceptor slightly different. This linker effect has been suggested by Best *et al.*[35] in their study of polyproline FRET in water solution. Although glycerol as a solvent makes the sample easier to handle, its dynamical complexity and its specific interactions with biomolecules make it difficult to compare the reorientation of the tethered dyes in the construct with their reorientation in water. The traces of Fig. 9(a) show clear indications of changes in conformation or relative dye orientation of the FRET-labeled single polyproline molecules. However, the present setup does not allow us to distinguish the contributions of these two factors. Nonetheless, the long periods with constant FRET efficiency indicate a near-absence of reorientations. We therefore believe that much of the rare conformational changes indicated by FRET efficiency changes are indeed due to reorientations of the dyes.

4. Conclusions

We have presented a single-molecule study of FRET-labeled all-*trans* polyprolines in glycerol. The conformations of the molecules were monitored *via* their FRET efficiency, used as a spectroscopic ruler. Our study, however, revealed the importance of dye orientation and reorientations. By following such reorientations of a single label in a partly immobilized molecule, one could study conformational changes without any need for a FRET measurement. The measured FRET distributions of the frozen constructs were considerably different from the theoretically expected distributions for isotropic orientations of donor and acceptor. These differences indicate a deviation from isotropy in the case of polyproline-6. For polyproline-20, the presence of molecules with a FRET-efficiency higher than the maximum for the stretched conformation suggests that the chain is not always completely stretched. We successfully demonstrated repetitive temperature-cycling of single oligopeptide molecules between 170 and 250 K. The time resolution, limited by the heating and cooling times, was of ten microseconds in the present experiments. The time in the high-temperature state and the temperatures can be tuned in a controlled fashion, to investigate different reaction pathways. Series of up to thousands of temperature-cycle measurements were recorded. They display long periods of constant FRET efficiencies, with rare and sudden efficiency jumps, presumably due to reorientations of one of the labels. These results make the temperature-cycle method particularly promising to study fast molecular dynamics at the single-molecule level. To better address relevant issues in the dynamics of biomolecules, such as protein folding, glycerol has to be replaced by a biocompatible buffer solution. This is the subject of current technical efforts.

Acknowledgements

We thank Dr Alexander Gaiduk for his help on Labview programming. We also thank Harmen van der Meer and Jos Disselhorst for their technical support. We acknowledge financial support by ERC (Advanced Grant SiMoSoMa). The work is part of the research program of the "Stichting voor Fundamenteel Onderzoek der Materie" (FOM) which is financially supported by the Netherlands Organization for Scientific Research (NWO).

References

1 M. Orrit and J. Bernard, *Phys. Rev. Lett.*, 1990, **65**, 2716–2719.
2 W. E. Moerner and M. Orrit, *Science*, 1999, **283**, 1670–6.
3 T. Ha, T. Enderle, D. F. Ogletree, D. S. Chemla, P. R. Selvin and S. Weiss, *Proc. Natl. Acad. Sci. U. S. A.*, 1996, **93**, 6264–8.
4 S. Hohng, C. Joo and T. Ha, *Biophys. J.*, 2004, **87**, 1328–1337.
5 X. Zhuang, L. E. Bartley, H. P. Babcock, R. Russell, T. Ha, D. Herschlag and S. Chu, *Science*, 2000, **288**, 2048–51.
6 N. K. Lee, A. N. Kapanidis, H. R. Koh, Y. Korlann, S. O. Ho, Y. Kim, N. Gassman, S. K. Kim and S. Weiss, *Biophys. J.*, 2007, **92**, 303–312.
7 B. Schuler, E. A. Lipman, P. J. Steinbach, M. Kumke and W. A. Eaton, *Proc. Natl. Acad. Sci. U. S. A.*, 2005, **102**, 2754–9.
8 M. Margittai, J. Widengren, E. Schweinberger, G. F. Schröder, S. Felekyan, E. Haustein, M. König, D. Fasshauer, H. Grubmüller, R. Jahn and C. A. M. Seidel, *Proc. Natl. Acad. Sci. U. S. A.*, 2003, **100**, 15516–15521.
9 A. K. Wozniak, G. F. Schröder, H. Grubmüller, C. A. Seidel and F. Oesterhelt, *Proc. Natl. Acad. Sci. U. S. A.*, 2008, **105**, 18337–18342.
10 D. Nettels, S. Mueller-Spaeth, F. Kuester, H. Hofmann, D. Haenni, S. Rueegger, L. Reymond, A. Hoffmann, J. Kubelka, B. Heinz, K. Gast, R. B. Best and B. Schuler, *Proc. Natl. Acad. Sci. U. S. A.*, 2009, **106**, 20740–20745.
11 T. Ha, A. Y. Ting, J. Liang, W. B. Caldwell, A. A. Deniz, D. S. Chemla, P. G. Schultz and S. Weiss, *Proc. Natl. Acad. Sci. U. S. A.*, 1999, **96**, 893–8.
12 A. A. Deniz, M. Dahan, J. R. Grunwell, T. Ha, A. E. Faulhaber, D. S. Chemla, S. Weiss and P. G. Schultz, *Proc. Natl. Acad. Sci. U. S. A.*, 1999, **96**, 3670–5.
13 E. Rhoades, E. Gussakovsky and G. Haran, *Proc. Natl. Acad. Sci. U. S. A.*, 2003, **100**, 3197–3202.
14 J. R. Lakowicz, *Principles of Fluorescence Spectroscopy*, Springer, 3rd edn, 2006.
15 R. E. Dale, J. Eisinger and W. E. Blumberg, *Biophys. J.*, 1979, **26**, 161–93.
16 J. Eisinger, B. Feuer and A. A. Lamola, *Biochemistry*, 1969, **8**, 3908–15.
17 K. A. Dill, S. B. Ozkan, T. R. Weikl, J. D. Chodera and V. A. Voelz, *Curr. Opin. Struct. Biol.*, 2007, **17**, 342–346.
18 R. Zondervan, F. Kulzer, H. van der Meer, J. A. J. M. Disselhorst and M. Orrit, *Biophys. J.*, 2006, **90**, 2958–69.
19 J. Sabelko, J. Ervin and M. Gruebele, *Proc. Natl. Acad. Sci. U. S. A.*, 1999, **96**, 6031–6036.
20 J. Kubelka, *Photochem. Photobiol. Sci.*, 2009, **8**, 499–512.

21 L. Stryer and R. P. Haugland, *Proc. Natl. Acad. Sci. U. S. A.*, 1967, **58**, 719–26.
22 K. Schröter and E. Donth, *J. Non-Cryst. Solids*, 2002, **307–310**, 270–280.
23 J. L. Dashnau, N. V. Nucci, K. A. Sharp and J. M. Vanderkooi, *J. Phys. Chem. B*, 2006, **110**, 13670–13677.
24 A. M. Klibanov, *Nature*, 2001, **409**, 241–246.
25 Serge N. Timasheff, in *Protein Stability and Folding*, ed. Bret Shirley, Humana Press, New Jersey, 1995, vol. 40, pp. 253–269.
26 M. Auton and D. W. Bolen, *Biochemistry*, 2004, **43**, 1329–1342.
27 F. Eker, K. Griebenow and R. Schweitzer-Stenner, *J. Am. Chem. Soc.*, 2003, **125**, 8178–8185.
28 K. Schroter and E. Donth, *J. Chem. Phys.*, 2000, **113**, 9101–9108.
29 V. Ivanov, M. Li and K. Mizuuchi, *Biophys. J.*, 2009, **97**, 922–929.
30 F. Ye, M. M. Collinson and D. A. Higgins, *Anal. Chem.*, 2007, **79**, 6465–6472.
31 Z. Sikorski and L. M. Davis, *Opt. Express*, 2008, **16**, 3660–3673.
32 R. Zondervan, F. Kulzer, S. Orlinskii and M. Orrit, *J. Phys. Chem. A*, 2003, **107**, 6770–6776.
33 R. Zondervan, F. Kulzer, M. Kol'chenko and M. Orrit, *J. Phys. Chem. A*, 2004, **108**, 1657–1665.
34 L. Watkins, H. Chang and H. Yang, *J. Phys. Chem. A*, 2006, **110**, 5191–5203.
35 R. B. Best, K. A. Merchant, I. V. Gopich, B. Schuler, A. Bax and W. A. Eaton, *Proc. Natl. Acad. Sci. U. S. A.*, 2007, **104**, 18964–9.
36 A. Paciaroni, S. Cinelli and G. Onori, *Biophys. J.*, 2002, **83**, 1157–1164.
37 R. Zondervan, F. Kulzer, G. C. G. Berkhout and M. Orrit, *Proc. Natl. Acad. Sci. U. S. A.*, 2007, **104**, 12628–12633.
38 E. Cornicchi, S. Cinelli, F. Natali, G. Onori and A. Paciaroni, *Phys. B*, 2004, **350**, E951–E954.
39 C. Chen, W. Z. Li, Y. C. Song and J. Yang, *J. Mol. Liq.*, 2009, **146**, 23–28.
40 A. Ansari, C. Jones, E. Henry, J. Hofrichter and W. Eaton, *Science*, 1992, **256**, 1796–1798.
41 R. Chelli, P. Procacci, G. Cardini and S. Califano, *Phys. Chem. Chem. Phys.*, 1999, **1**, 879–885.
42 M. Gonnelli and G. Strambini, *Biophys. J.*, 1993, **65**, 131–137.